GeoPlanning
Journal of Geomatics and Planning
Geoplanning: Journal of Geomatics and Planning, Vol. 12, No. 1, 2025, 79 - 94

e-ISSN: 2355-6544

Received: 23 December 2024;
Revised: 28 January 2025;
Accepted: 28 February 2025;
Available Online: 14 May 2025;
Published: 26 May 2025.

Keywords:
SAR Imagery, DinsSAR, Deformation, Subsidence, Uplift, Fault

*Corresponding author(s)
email: imanuela.indah@gmail.com

Original Research Open access

Post-Seismic Surface Deformation of The Tarakan Earthquake in 2015 Using the DInSAR Technique

Imanuela Indah Pertiwi [1]*, Trismahargyono [2], Marniati [3], Joshua Purba [4]

1. *Kendari Class IV Geophysical Station – BMKG, Indonesia*
2. *Center of Earthquake and Tsunami – BMKG, Indonesia*
3. *Makassar Region IV Meteorology, Climatology, and Geophysics Center – BMKG, Indonesia*
4. *Gowa Class II Geophysical Station – BMKG, Indonesia*

DOI: 10.14710/geoplanning.12.1.79-94

Abstract

Deformation can help predict the presence and severity of an earthquake. SAR image data can be used to calculate post-seismic surface deformation using the InSAR and DInSAR methods. DInSAR (Differential Interferometric Synthetic Aperture Radar) is a well-established technology for monitoring subsidence and uplift with millimeter precision. This study uses SAR imagery to detect surface deformation caused by a magnitude M 6.1 earthquake on December 21, 2015, at 01:47:37 WIB in Tarakan Regency, North Borneo. The data used is Sentinel-1 satellite imagery in SLC (single-look complex) format, with a master image from December 18, 2015 (3 days before the earthquake), and a slave image from January 11, 2016 (21 days after). The interferogram generated by the Tarakan earthquake shows deformation patterns radiating in three directions: northeast, southeast-southwest, and southwest-northwest. Tarakan City, located south-southwest of the epicenter, experienced the highest subsidence deformation of 0.001–0.035 meters. On December 21, 2015, the Tana Tidung I Regency area, 33 kilometers southwest of the epicenter, showed the highest uplift deformation (0.019–0.079 meters). The largest uplift in Tana Tidung II Regency (0.069 meters), about 10 kilometers north of the epicenter, occurred near the fault zone. Surface deformation due to the Tarakan earthquake contributes to seismic hazard assessment in North Borneo and indicates other locally active faults. Uplift to the east and subsidence to the west of the epicenter suggest an oblique-normal fault, with dominant strike-slip motion and normal (downward) fault blocks to the west.

1. Introduction

Seismotectonic processes triggered by plate movements produce seismic and volcanic activity (Hanifa et al. 2019). Earthquake events typically alter the shape or position of the earth's surface (deformation) (Panuntun et al. 2018). An earthquake typically causes the surrounding earth's crust to deform in both vertical and horizontal directions (Sari et al. 2014). This deformation consists of three components: change in location (translation), change in orientation or direction (rotation), and force (strain and stress). Deformation can be a major factor in determining the presence and severity of an earthquake (Puspita et al. 2024). Deformation caused by a big earthquake has a severe influence on the infrastructure and buildings above it. It is commonly recognized that all macro earthquakes (e.g. events whose M > 3.0) cause crustal deformation, but only earthquakes over a particular magnitude usually cause surface rupture (Gürpinar et al. 2017). The amount of deformation can be calculated from SAR picture data (Cahyaningrum, 2024) using the InSAR and DInSAR methods. The worth of surface changes can be determined by subtracting or differential InSAR (DINSAR) from three or more radar pictures or by applying a topographic surface model (Kurniawan et al. 2016). DInSAR (Differential Interferometric Synthetic Aperture Radar) is a well-developed technology for measuring subsidence with excellent precision in millimeters (Islam et al. 2017). This technique employs more than two radar pictures (multitemporal radar images), resulting in temporal decorrelation and atmospheric dishomogeneities that affect interferogram quality.

The Tarakan earthquake is a rare occurrence, as Borneo is Indonesia's sole island with a low frequency of seismic activity. However, the Tarakan earthquake of magnitude M 6.1 damaged several houses, including two (two) houses in Selumit Village, Central Tarakan Subdistrict Beach, four (four) houses damaged and experiencing landslides in Juata Kerikil Village, and one (one) house under construction that was damaged or collapsed in Juata Laut Village (North Borneo Regional Disaster Management Agency, 2016). Based on damage data from different sub-districts affected by the earthquake, this study uses SAR satellite image data to evaluate vertical surface deformation information (Souza et al. 2024; Gourmelen et al. 2010; Bedini 2020) in the form of subsidence and uplift produced by the Tarakan earthquake on December 21, 2015.

In this study, SAR pictures were utilized to detect surface deformation induced by an earthquake that struck most of North Borneo Province on Monday, December 21, 2015, at 01:47:37 a.m., including Tarakan, Nunukan, and Tanjung Selor. The BMKG (Meteorology, Climatology, and Geophysics Agency) analysis indicates that this earthquake has a magnitude of 6.1 (update). The earthquake's epicenter was on land at coordinates 3.61°LS and 117.67°BT, or 29 kilometers northeast of Tarakan City in North Borneo, with a hypocenter depth of 10 kilometers. Earthquake shocks were felt in various locations, including Tarakan and Nunukan IV-V MMI and Tanjung Selor III-IV MMI. The earthquake that occurred was an intraplate-type shallow crustal earthquake with a shallow hypocenter caused by active fault activity (Center of Earthquake and Tsunami BMKG, 2016). The earthquake has a land epicenter does not have the ability to create a tsunami.

Lu et al. 2025 successfully identified the fault movement that caused the 2025 Dapu earthquake, as indicated by the presence of ground cracks and water ejection in the DInSAR analysis results. Research on the use of the DInSAR method in determining potential seismic hazard areas has been conducted on the 2017 Poso earthquake, the area in the Southern part of North Lore District is dominated by maximum uplift deformation values and subsidence deformation values which are quite large, causing many buildings to sufferlight to heavy damage (Puspita et al. 2024). The DInSAR method was also conducted to determine surface defromation and its implications for land degradation after the 2021 Flores earthquake (Purba et al. 2024) on Kalatoa island. The results showed land subsidence of up to 12 cm in Garaupa Raya Village and land uplift of up to 10 cm in Lembang Mate'ne Village. The total area that experienced land subsidence was 39.4 km² (50.50%), while the area that experienced land uplift was 38.2 km² (49.02%). Calvet et al. 2023 research proves that the DinSAR technique to be useful and powerful for the observation and analysis of surface deformation caused by the release of stress during the Mw 8.3 Illapel earthquake. It proved to be an efficient tool to detect and map the surface deformation with high spatial resolution in an approximate area of 20,000 km².

There has been little research into the potential earthquake hazard on Borneo Island. The island of Borneo has long been known as one of the areas in Indonesia that is safe from earthquake disasters. Previous research on the Tarakan earthquake on December 21, 2015 identified micro-faults that caused the earthquake. The results of this research show the direction of fault movement based on the distribution of aftershocks (Sriyanto et al. 2016). This research combines Differential Interferometric Synthetic Aperture Radar (DInSAR) analysis, focal mechanism analysis, and correlation with local geological conditions. The results of SAR image processing were analysed to determine the value of surface deformation due to the Tarakan earthquake. The surface deformation that occurred in the area around the earthquake can provide information related to seismic hazard in the North Borneo region, as well as identify the characteristics of the fault that caused the Tarakan earthquake. The results of this study are expected to be a reference in improving future earthquake preparedness strategies in the North Borneo region. The identification of fault characteristics using the DInSAR method can be a verification of the results of previous research. The surface deformation caused by the earthquake is a visual representation of the fault movement that causes the earthquake.

2. Data and Methods

2.1. Research Location

This research is being conducted in the province of North Borneo, which has geographical coordinates of 3°18' 00"– 4°24' 00" North Latitude and 115°30'00"–118°00' 00" East Longitude. The North Borneo region is made up of one city and four regencies: Bulungan, Malinau, Nunukan, Tana Tidung, and Tarakan City. The study focused on locations in North Borneo province that experienced surface deformation following the December 21, 2015 earthquake.

2.2. The Geological Structure of Borneo Island and Seismo-Tectonics of North Borneo

Borneo formed through the accretion of microcontinental fragments, ophiolite terranes, and island-arc crust onto a Paleozoic continental core during the Mesozoic era. At the beginning of the Cenozoic era, Borneo formed part of the promontory of Sundaland, which was partly separated from the Asian mainland by the proto-South China Sea (Balaguru et al. 2003). The Barito Basin in southern Borneo is underlain by accreted crust from the Meratus Mountains in the east and Schwaner bedrock of continental origin in the west, and contains a thick and well-exposed succession of Cenozoic sediments (Witts et al. 2012). To the north, the Kutai Basin is limited by accreted crust from the Kucing Plateau (part of the Central Range) and Mangkalihat continental bedrock to the west and north. Tarakan Basin is farther northerly than Kutai and is surrounded by the Dent-Semporna accreted crust, the Sekatak-Berau Plateau, and the Mangkalihat continental basement. The links between these basement terranes are not entirely clear. The Tarakan Basin is located offshore North-East Borneo Island, in a structurally complex zone of continental convergence involving subduction of Northern Sulawesi (Hall, 2013; 2019); Watkinson et al. 2017).

The dominant characteristic of the Tarakan Basin is the presence of fine to coarse-grained clastic sedimentary rocks with carbonate deposits (Hendardi et al. 2024). The temporal and spatial evolution of Neogene deformation in the shelf-edge to upper slope region of the Tarakan Basin reflects the interaction between variations in sediment accumulation rates, the progradation of deltaic sedimentary wedges, mobile shale flows and the growth and linkage of extensional faults. Evidence of Neogene deformation in the Tarakan Basin includes growth normal faults, shale rollers and anticlines, mud pipes and volcanoes. Deformation was controlled by mobile shale flow across varying dips in the base of the mobile shale surface, gravitational loading and gliding. Growth faults formed through tip propagation and segment linkage, as well as late-stage tip retreat and reactivation. The dipping of the base of the mobile shale controls the position, timing and evolution of the growth faults and their associated depocentres (Erdi et al. 2023). The Barito, Kutai and Tarakan basins shared a similar tectonic history during the Tertiary, characterized by an extensional regime in the Paleogene and a compressional regime in Neogene and Pleistocene time. However, their tectonic origins and styles are dissimilar. Several of the Borneo deltas (Tarakan, Baram, West Luconia) exhibit large coupled extensional-compressional deformation systems (Gorsel, 2018). The Kutai Basin formed during the Early Tertiary period, filling up with clastic sediments from west to east (Permana et al. 2018). The Geological Map of North Borneo (Figure 1) shows that the majority of the region is made up of alluvium deposits, particularly in Nunukan, Tana Tidung, and parts of Tarakan City. Other areas of Tarakan City include the Sejau Formation, which contains sedimentary, clastic, and flish rock formations (Indonesia Geospasial, 2020).

The eastern half of Borneo Island has complicated tectonic conditions, making it the most earthquake-prone area on the island. The existence of many descending fault geological formations, as well as several horizontal fault structures, contributes to the zone's earthquake vulnerability. Three horizontal faults run across the Nunukan-Tarakan zone and its environs. To the south are two southwest-southeast trending faults, the Mangkalihat Fault Zone and the Maratua Fault Zone. The Mangkalihat Fault Zone is a continuation of the Palu

Koro Fault, which runs near Tanjung Redep. The occurrence of the Maratua Fault Zone is significant because its terminus is located in the ocean near Tanjung Selor town. Meanwhile, to the north of Tarakan Island, the Sempurna Fault Zone extends from the Sulawesi Sea to Sabah, Malaysia, crossing the area around Sebatik Island. Borneo Island also contains the Tarakan and Meratus faults. The Tarakan, Mangkalihat, and Meratus faults are more than 100 kilometers long and have the potential to create earthquakes of magnitude 7. The Tarakan horizontal fault may be seen in the northern portion of the island (Figure 2), which extends from the mainland to the offshore. The Mangkalihat fault, a horizontal fault, is located on the east coast of Borneo Island. In the southern half of Borneo Island, there is a stepping fault zone known as the Meratus Fault, which runs from north-east to south-west (National Center for Earthquake Studies, 2017). However, it remains unclear which fault structure caused the earthquake that struck the majority of East Borneo on December 21, 2015.

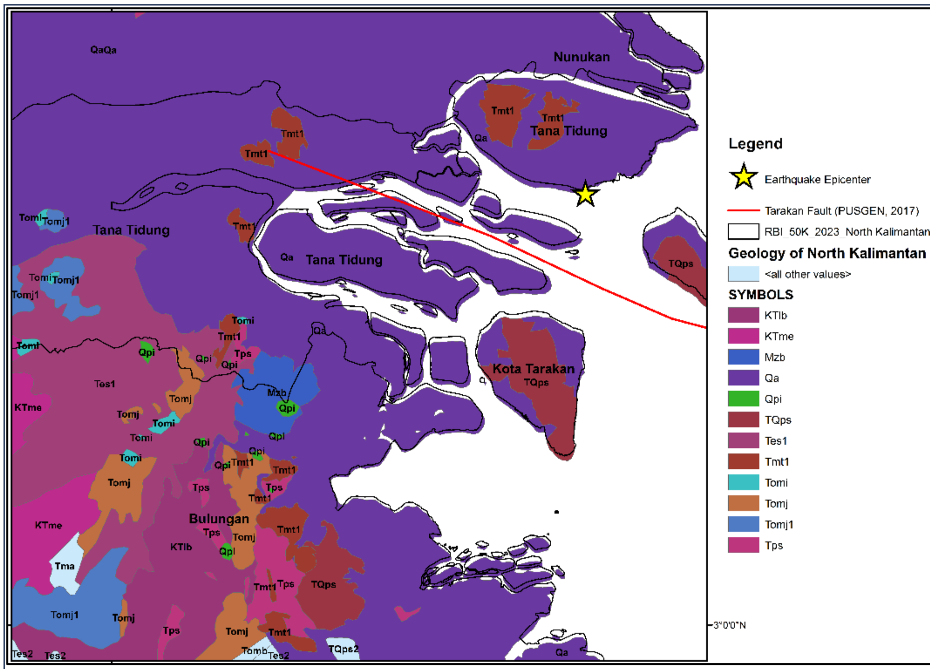

Information:

KTib : Long Bawan Formation (fish, coastal, lagoon, clastic, sedimentary structure)
KTme :Mentarang Formation (sedimentary structure, clastic, fish, neritic, continental slope)
Mzb :Bengara Formation (sedimentary structures, clastics, fish, deep sea)
Qa : Alluvium deposits (sedimentary structures, clastics, alluvium)
Qpi :Quarter Intrusions (intermediate intrusive rocks, breakthrough igneous rock bodies)
TQps : Sajau Formation (sedimentary structures, clastics, terrestrial fish, fluvial, delta)
Tes1 : Sedimentary, clastic, littoral sandstone.
Tomi : Breakthrough rock (extrusive rock, intermediate, lava, volcanic)
Tomj : Karamuan Formation (limestone sediments, reefs)
Tomj1 : Barley volcanic rocks (intermediate extrusive rocks, volcanic polymics)
Tps : Sinjin Formation (volcanic pyroclastic intermediate extrusive rock)

Source: (Indonesia Geospasial, 2020)

Figure 1. North Borneo's Geological Structure

Tarakan, North Borneo, has a very short history of significant earthquakes. Tarakan City has seen four significant and devastating earthquakes. The Tarakan earthquake on April 19, 1923, had an estimated magnitude of 7.0. The earthquake reached a magnitude of VII–VIII MMI, inflicting damage to several homes and ground cracks. Second, on February 14, 1925, the Tarakan earthquake caused very powerful shaking with an intensity scale of VI–VII MMI, causing numerous buildings to be damaged. The third was the Tarakan earthquake on February 28, 1936, which had a magnitude of 6.5 and damaged a number of structures; (North Borneo Regional Disaster Management Agency, 1956) the fourth was the Tarakan earthquake on December 21, 2015. According to the focal mechanism analysis from the Global CMT database (Figure 3), the Tarakan earthquake had a normal-oblique fault source mechanism. Focal mechanisms of earthquakes are essential for identifying fault planes and characteristics of faults (Purba et al. 2025). These characteristics are determined by analysing the strike, dip and slip parameters of an earthquake, which helps to identify its source and cause. The history of Tarakan earthquakes of such magnitude suggests that the region contains active tectonic formations.

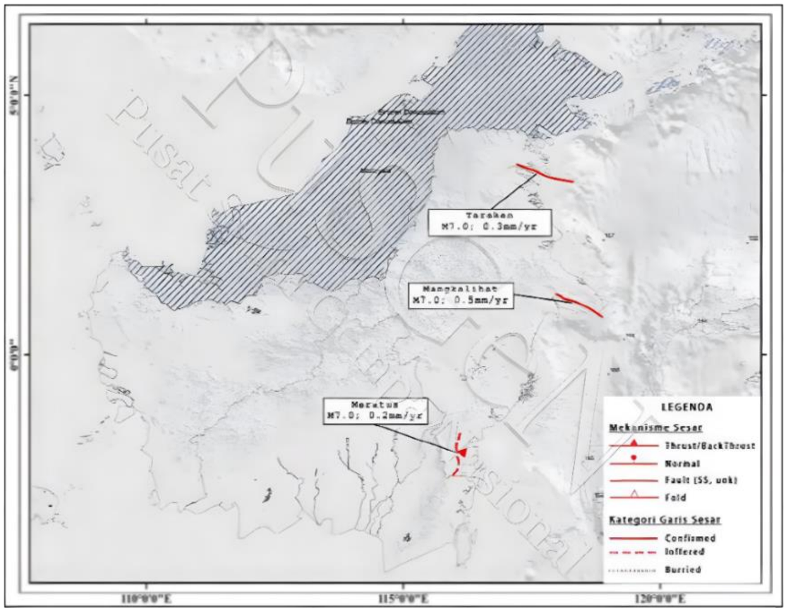

Source: (National Center for Earthquake Studies, 2017).

Figure 2. Fault Structure in Borneo

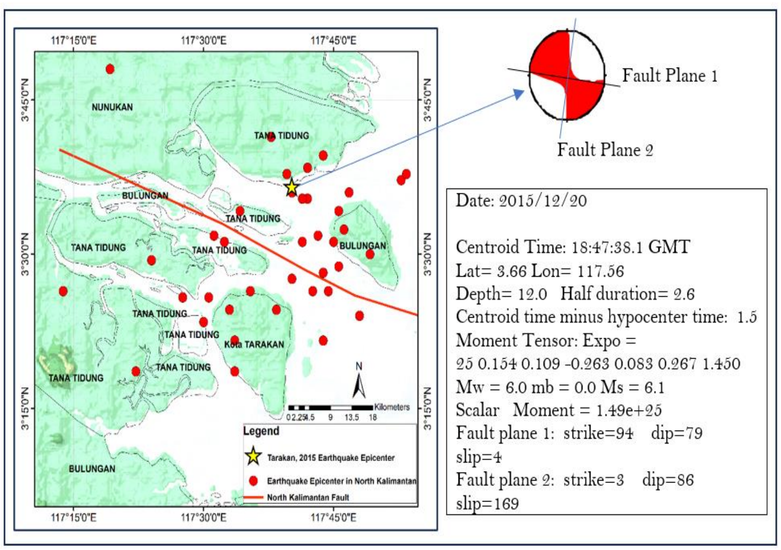

Source: BMKG Data Catalog and Global Centroid-Moment Tensor Catalog Web Search

Figure 3. Spatial Distribution of the North Borneo Earthquake Epicenters Period 1980 – 2021 and Focal Mechanism of the Tarakan Earthquake

2.3. SAR Image Data

SAR is a microwave-based imager that can penetrate clouds. Active SAR sensors send pulses and listen for echoes. These echoes are captured in terms of phase and amplitude. The phase is utilized to calculate the distance between the sensor and the target, while the amplitude provides information about the roughness and dielectric constant of the target. Several factors influence the interferogram, including earth curvature, topographic effects, atmospheric delay, surface motion, and noise (Castaneda et al. 2011). Sentinel-1 SAR photos can identify changes in the earth's surface on a centimeter scale with adequate processing. In addition, it can be used to assess volcanic deformation, subsidence, landslides, and earthquakes. SAR data is a digital record of waves (energy) emitted by a radar sensor from a satellite to the Earth's surface and reflected back (backscattering) to the satellite's receiving sensor.

The Sentinel-1 satellite's SAR sensor transmits a C-band signal with a wavelength of 5.6 cm. The wavelength of the signal influences its penetration ability; hence, it is critical to understand the wavelength of the sensor when working with SAR datasets. C-band SAR signals penetrate further into the canopy or surface (NASA's Earth Science Data System) than X-band signals, but not as deeply as L-band SAR signals, which have a wavelength of approximately 25 cm and are better able to penetrate the canopy and return signals from the forest floor. Different wavelengths are also sensitive to various degrees of deformation. To detect very minor changes in a relatively short period of time, signals with shorter wavelengths (such as the X-band) are necessary. Signals of shorter wavelengths, on the other hand, are more prone to decorrelation caused by minor changes in surface conditions, such as vegetation development. Longer wavelengths (such as the L-band) may be required for slower processes that detect motion over longer time periods. The C-band's central position can detect small changes in a short period of time, but it is not as sensitive to small changes as the X-band or as capable of monitoring surface dynamics under the canopy as the L-band.

To detect surface deformation induced by an earthquake, at least two SAR photos of the same object taken at different times are required: after and before the earthquake. The SAR picture at time t before the earthquake is referred to as the master, whereas time t_1 after the earthquake is referred to as the slave. The phase value is acquired from both the first and second pass images (Figure 4). If the first and second trajectory images have a phase difference, the interferogram will show displacement fringes. The interferogram has two basic fringes: displacement fringes induced by shifting topographic surfaces and topographic fringes caused by topographic forms (Campbell et. al 2011).

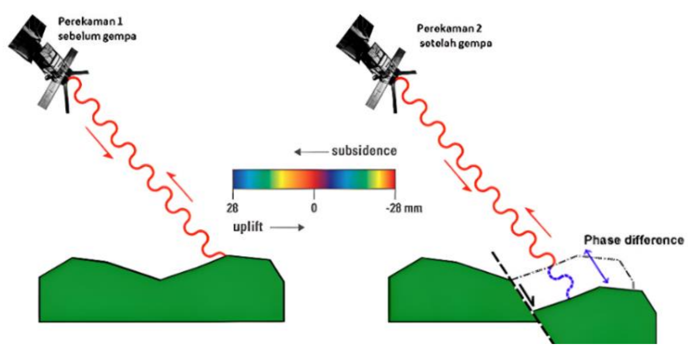

Source: Analysis, 2025

Figure 4. Two SAR Imaging Trajectories Obtained at Time t (Before the Earthquake) and t_1 (After the Earthquake) will Provide Ground Surface Movement with a Phase Shift of the SAR Signal Caused by the Earthquake).

Sentinel-1 satellite imagery in single-look complex (SLC) format, also known as 2017 Copernicus Sentinel data (ASF HyP3 Sentinel-1 Burst InSAR Product Guide), consists of two satellites, Sentinel-1A and Sentinel-1B, each carrying a C- band Synthetic Aperture Radar (SAR) instrument for round-the-clock global photography, eventhrough cloud cover. Both satellites orbit in tandem, 180° apart. Each satellite may repeat every 12 days, and Sentinel-1 can repeat every 6 days thanks to the constellation of two satellites (Azhari et al. 2020; Braun et al., 2020 Téllez-Quiñones et al. 2020) Sentinel-1 has four observation modes, the main one on land being the Interferometric Wide Swath (IW) mode, which has a spatial resolution of around 5 m x 20 m (Islam et al. 2017).

Surface deformation induced by an earthquake can be detected if there is a phase difference between the master (the first picture acquired) and slave (the second image acquired), as seen in the interferogram created by multiplying the amplitude by the phase difference of the signals (Hogenson et al., 2020). In this study, two Sentinel-1 SAR pictures were utilized to assess surface deformation induced by the Tarakan earthquake on December 21, 2015. The master data was recorded on December 18, 2015, three days before the earthquake, and the slave data was recorded on January 11, 2016 (21 days later).

2.4 DInSAR Method

Differential interferometric synthetic aperture radar (DInSAR), as an extension of InSAR, has become a mature method for monitoring deformations in mining areas (Manconi, 2021; Jiang et al. 2023; Govil et al. 2023). DInSAR techniques can be used to monitor topographic change, surface deformation or terrain displacement induced by different phenomena, like earthquakes or seismic activity, magma accumulation due to volcanic lava flow, and particularly, glacier or ice-flow dynamic (Téllez-Quiñones et al. 2025) using two SAR images. The basic purpose of DInSAR is to extract the full phase caused exclusively by deformation while deleting or minimizing other contributing components. If a topographic surface module serves as a reference or if three or more radar images are employed, differential InSAR can be used to determine the changes. The DInSAR approach relies on DEM (Digital Elevation Model) data to execute differential 2-pass interferometry operations. The DEM used is GLO-30 (Fahrland et al. 2020), with an initial pixel spacing of 1 arcsecond (about 30 meters). The Copernicus DEM Glo-30 is a global digital surface model (DSM) built on the WorldDEM. WorldDEM is based on radar satellite data gathered by the TanDEM-X mission, which has been modified to flatten water bodies, provide steady river flows, and change beaches, coasts, and distinguishing features. The phase information contained in the interferograms of the two SAR observations taken at different periods comprises topography, orbital drift, surface deformation, atmospheric influences, and thermal noise (Castaneda et al. 2011). This interferogram will show whether there is land subsidence or rising in a specific area. Phase wrapping is the result of calculating the height difference that depends on the phase difference between the interferogram intervals (-π, π).

The phase change of the signal (Δφ) (Equation 1) is affected by the wavelength (λ), displacement (δR), and phase change due to the difference in atmospheric conditions (Castaneda et al. 2011) during acquisition by the two radars (α). The phase difference value can be formulated by the following equation (Equation 2):

$$\Delta\varphi = 4\pi\frac{\delta R}{\lambda} + \alpha \quad \text{(Equation. 1)}$$

$$\Delta\varphi = \Delta\varphi_{flat} + \Delta\varphi_{elevasi} + \Delta\varphi_{deformasi} + \Delta\varphi_{atmosfer} + \Delta\varphi_{noise} \quad \text{(Equation. 2)}$$

where $\Delta\varphi_{flat}$ is the phase due to topographic influences. Using the above equation, the $\Delta\varphi_{flat}$ (Equation 3) was computed using:

$$\Delta\varphi_{flat} = -\frac{4\pi}{\lambda}\,\frac{B_n}{R t a n t a n\,\theta} \quad \text{(Equation. 3)}$$

where $\Delta\varphi_{elevasi}$ is the phase influenced by height. Using the above equation, the $\Delta\varphi_{flat}$ 9 (Equation 4) was computed using:

$$\Delta\varphi_{elevasi} = -\frac{\Delta q}{sinsin\,\theta}\cdot\frac{B_n}{R}\cdot\frac{4\pi}{\lambda} \quad \text{(Equation. 4)}$$

where $\Delta\varphi_{atmosfer}$ is the phase due to atmospheric influences. Using the above equation, the $\Delta\varphi_{flat}$ (Equation 5) was computed using:

$$\Delta\varphi_{atmosfer} = \frac{4\pi}{\lambda}\,d \quad \text{(Equation. 5)}$$

with ($B_{n)}$ is the baseline perpendicular to the slope (perpendicular baseline) (m), (R) is the radar distance to target (m), and (θ) is the angle of incidence (degrees).

This study used SNAP software for Sentinel-1 SAR image data processing and visualization, Google Earth software for virtually visualizing research data on the earth's surface, and ArcGIS software version 10.8 for raster data operations and data representation. The majority of Sentinel-1 image data is processed using the SNAP program (ESA, 2021). Furthermore, data is visualized and represented using Google Earth and ArcGIS 10.8 software. The picture data processing yielded a surface deformation map (LOS displacement) from the December 21, 2015 Tarakan earthquake.

3. Result and Discussion

3.1. Interferogram Phase

The phase interferogram is able to show areas that experienced surface resolution due to the Poso earthquake on May 29, 2017 (Puspita et al. 2024). Processing the SAR image observation data yields color-differentiated interferograms displaying the phase shifts of radar waves before and after the earthquake (Figure 5). The colorful contours show the interference fringes between the two datasets. The distance between each interference fringe denotes ground motion. The phase difference in the interferogram is represented by blue-to-pink pixels in the positive phase and blue-to-yellow pixels in the negative phase. The denser the interferogram fringes, the higher the strain on the ground during the earthquake. The Tarakan earthquake's interferogram is centered on the main earthquake and extends north-northeast, southeast-southwest, and southwest-northwest. The contrast of the interferogram color repetition (fringe) is not clearly evident, which could be due to air noise, topography influences, or the region's dense vegetation. Although the margins are not easily apparent, the distorted portions can still be distinguished.

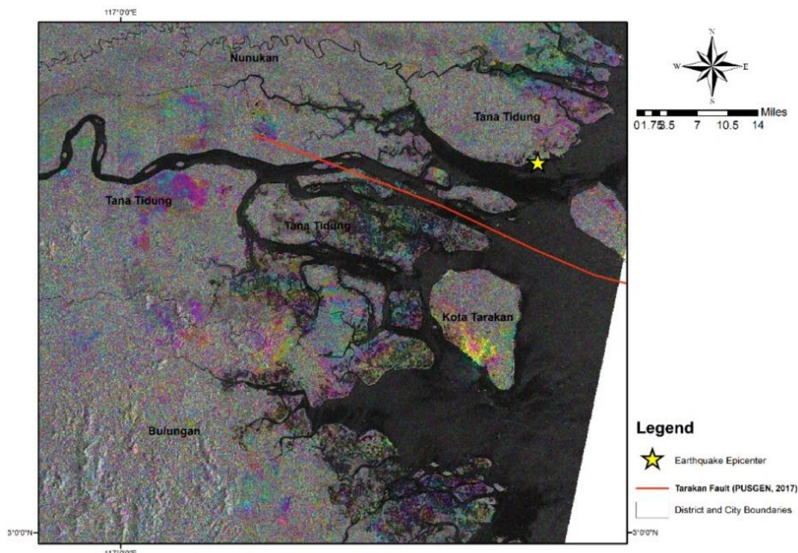

Source: Analysis, 2025

Figure 5. Tarakan Earthquake Interferogram, December 21, 2015

3.2. Coherence Value Map

Coherence value ranges from 0 to 1, with higher values indicating better interferogram quality. The interferometry procedure is considered good and accurate if the image's coherence value ranges between 0.5 and 1.0. If the value is less than 0.5, the image produced from the interferometry process still contains useful information, (Kurniawan et al. 2016) but the image with the coherence value also exhibits an increase in noise level proportionate to the smaller coherence value. Areas with high coherence will have clear color contours, whereas freckles areas show very low coherence and noise. Typically, a surface that remains constant throughout the difference time picture acquisition produces a very high coherence (Jaya et al. 2021). An interferogram's coherence is affected by several factors, including the angle and orientation of the topographic slope (steep slopes lead to low coherence), the nature of the land, the time spacing of the images (longer time intervals lead to lower coherence), and the baseline.

DOI: 10.14710/geoplanning.12.1.79-94

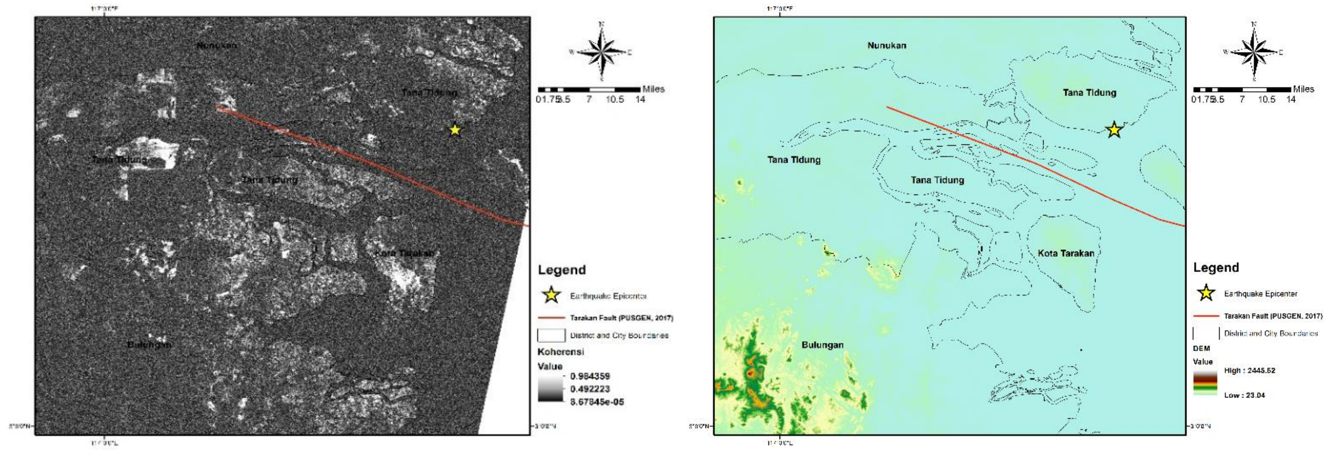

(a) (b)

Source: Analysis, 2025

Figure 6. (a) SAR Coherence Distribution Map (b) DEM (Digital Elevation Model) Map of North Borneo

Figure 6(a) depicts the range of coherence values in the North Borneo region, namely the areas surrounding the Tarakan earthquake, with coherence values ranging from 0.4 to 0.9. Topographic characteristics and forest density influence both high (white) and low (dark gray) coherence values in the North Borneo region (Figure 6(b)). Due to the region's flat topography, white dominates the coherence map in places near the epicenter. Some locations with low coherence values (less than 0.4) are generated by sentinel imaging that employs a C-band with a wavelength of 5.4 cm; therefore, the radar waves are insufficient to penetrate the vegetation canopy, resulting in poor interferogram accuracy. Areas with coherence greater than 0.8 are situated northeast, southwest, north, south, west, and southeast of the main earthquake, as shown by white pixels. These findings indicate that these places are largely flat with no substantial topographical changes, resulting in numerous reflections of radar signal interference. If deformation happens, areas with high coherence values will produce more interferograms, with fringe lines that are more regular than those with low coherence values.

3.3. Deformation Phase (Wrapped and Unwrapped Phase)

The resulting deformation value remains a deformation phase (wrapped phase) with both negative and positive phase values. Figure 7(a) depicts the deformation phase throughout the co-seismic period of the main Tarakan earthquake, with an updated magnitude of M 6.1 (yellow star). Negative phase values indicate subsidence-related deformation, which is illustrated in red. Positive phase values indicate areas of uplift, as illustrated in blue (Cahyaningrum, 2024). Areas that are white in color, as well as phase points, are often very stable and do not undergo modifications or deformation. The deformed areas are all located some distance from the main earthquake.

To measure the amount of deformation in a metric, a computation must be performed using the displacement of the earth's surface formula along the Line of Sight (LOS) sensor, as shown in (Equation 1). After unwrapping the interferogram, as shown in Figure 7(b), the area deformation pattern can be determined even if it is still in phase units. Line of Sight (LOS) analysis indicates the satellite's flying direction. If the value is positive, it means that the axis is stretched towards the satellite, indicating land subsidence. If the result is negative, it indicates that the axis is shorter towards the satellite, implying an increase in land level (uplift) (Cahyaningrum, 2024). Based on this image, the largest land surface rise (uplift) deformation value is 0.117618 meters, which is highlighted in red around the main earthquake. Areas undergoing ground subsidence deformation are depicted in blue, with a maximum deformation value of 0.0649612 meters, which is also near the main earthquake. The deformation was directly tied to aftershock activity following the primary earthquake.

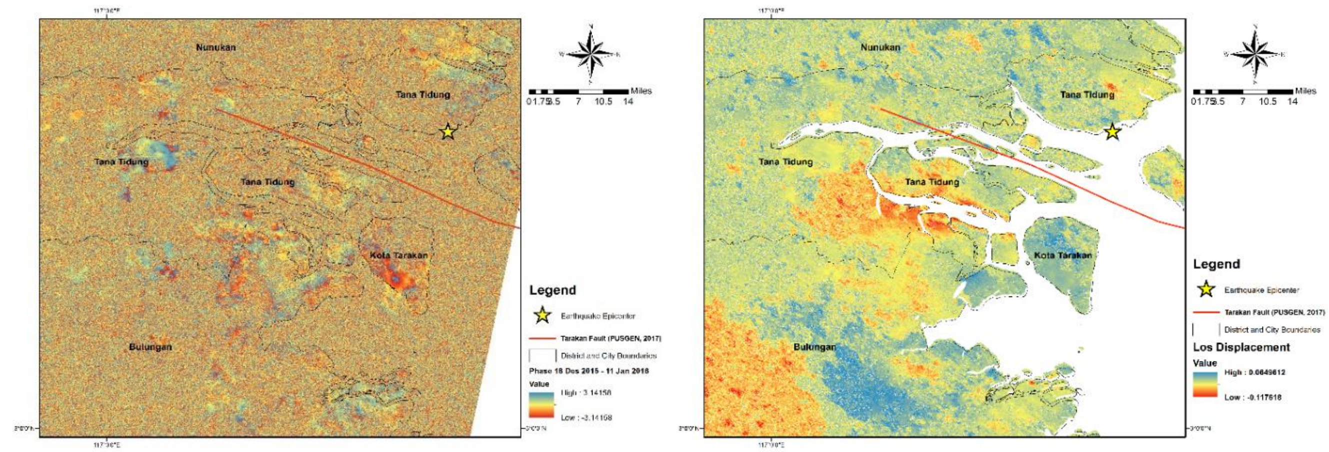

(a) (b)

Source: Analysis, 2025

Figure 7. (a) Tarakan Earthquake Deformation Phase December 21, 2015 (b) Los Displacements (Changes in Deformation) Related to the Tarakan Earthquake on December 21, 2015.

The Loss Displacement Map in Figure 7(b) depicts the magnitude of deformation change data in various districts and cities in North Borneo following the Tarakan earthquake on December 21, 2015. Tarakan City, located to the south of the main earthquake (yellow star), appears on the map as blue to yellow, suggesting that the deformation change that happened was subsidence (lowering of the land surface), with the deformation value nearly reaching its maximum. Tana Tidung Regency, located just southwest of the main earthquake, is primarily colored red, suggesting that there is deformation change in the form of uplift (an increase in land level) with a value close to its maximum. The same pattern is seen in the Tana Tidung Regency area, which is directly north of the main earthquake, with yellow to red indicating a change in maximum uplift deformation. Nunukan Regency, located northwest of the main earthquake, displays blue to light orange, suggesting changes in subsidence deformation. The Bulungan Regency area, located southeast of the major earthquake (Bunyu Island), appears to be dominated by yellow to orange colors, indicating that uplift deformation has occurred in this location.

3.4. Cross Section Deformation

To estimate the deformation value in the areas surrounding the epicenter (Gabriel et al. 1989) of the Tarakan earthquake on December 21, 2015, a vertical cut (cross-section) was performed in each district area to demonstrate the influence of changes in deformation. The cross section formed generates a cross-section graph, with the Y axis representing the value of changes in land surface (deformation) in meters and the X axis representing the length of the cross section in the Regency area in kilometers. According to (Petersen et al. 2011), the risk of ruptures occurring off-fault is significantly lower than the risk close to the fault. However, the data show that adjacent faults at least 10 km (km) away from the principal fault and with a meter-scale offset on the primary fault can cause displacements of up to 35 cm (cm).

The Tarakan City area, located around 22 kilometers south of the earthquake's epicenter (Figure 9) exhibits subsidence deformation ranging from 0.001-0.035 meters in the northwest-southeast cross section. The graph along the cross section depicts the subsidence deformation that dominates the Tarakan City area, namely the area directly south-southwest of the earthquake's epicenter.

The Tana Tidung I Regency area, located 33 kilometers southwest of the earthquake epicenter, has uplift deformation ranging from 0.019 to 0.079 meters in the northwest-southeast cross section (Figure 10). Uplift deformation dominates this region, with the highest value displayed by the graph occurring directly southwest of the location of the Tarakan earthquake on December 21, 2015. Figure 11 depicts a cross-section graphic showing the northwest-southeast cross-section in the Bulungan Regency area, which is located around 11 kilometers southeast of the earthquake epicenter. Based on graphic pictures, uplift deformation dominates this area, with major deformations ranging from 0.008 to 0.075 meters. The highest uplift deformation value occurs in the southeastern Bulungan region, or precisely to the southeast of the earthquake's epicenter.

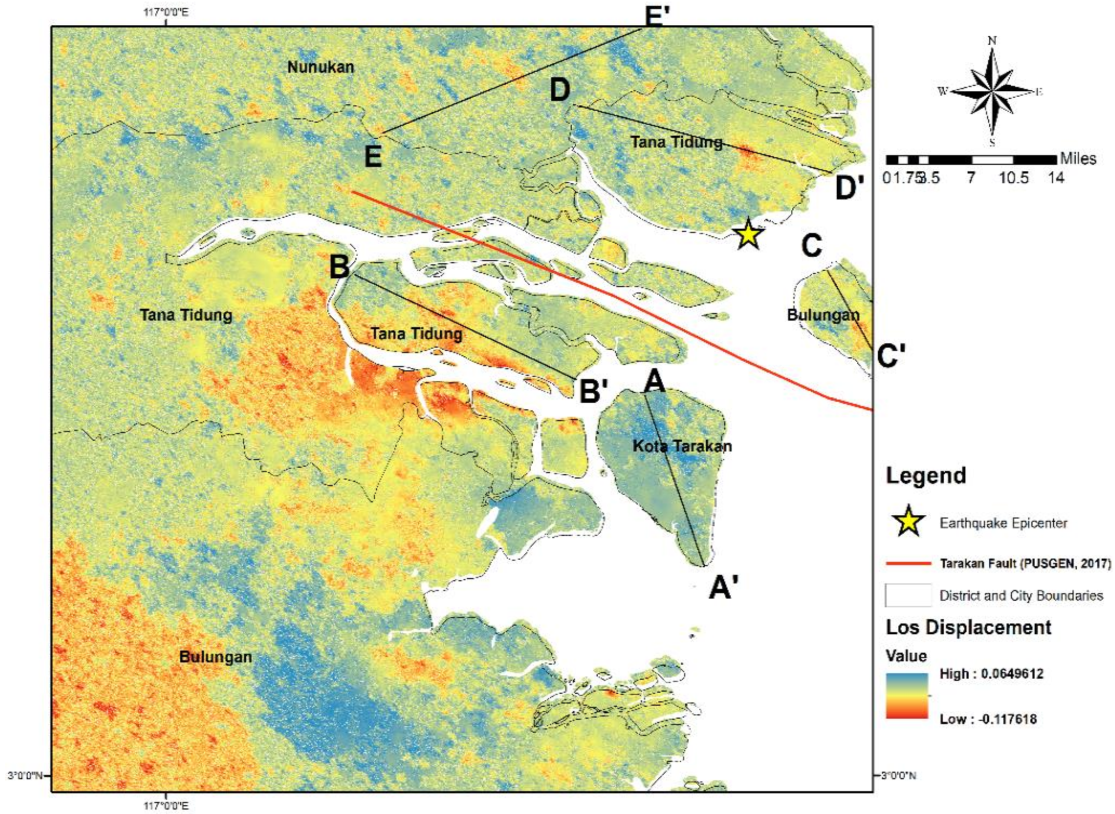

Source: Analysis, 2025

Figure 8. Cross Sections were Conducted in each District Region Near the Epicenter of the Tarakan Earthquake on December 21, 2015

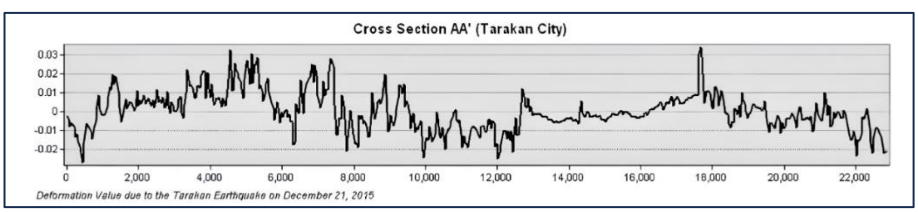

Source: Analysis, 2025

Figure 9. Vertical Cross-section Graph of AA' at Tarakan City

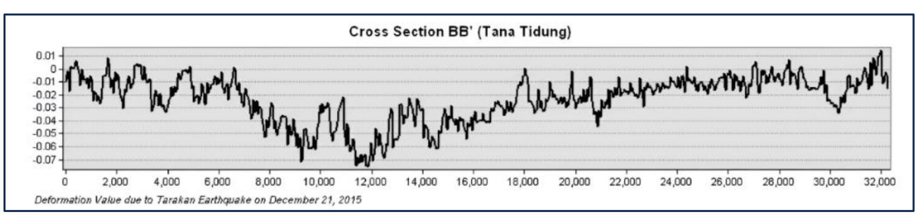

Source: Analysis, 2025

Figure 10. Vertical Cross-section Graph of BB' in Tana Tidung I Regency

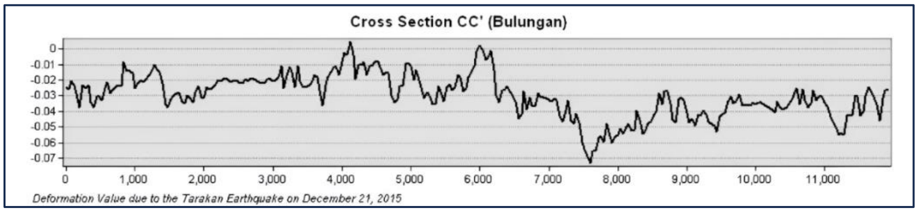

Source: Analysis, 2025

Figure 11. Vertical Cross-section Graph of CC' in Bulungan Regency.

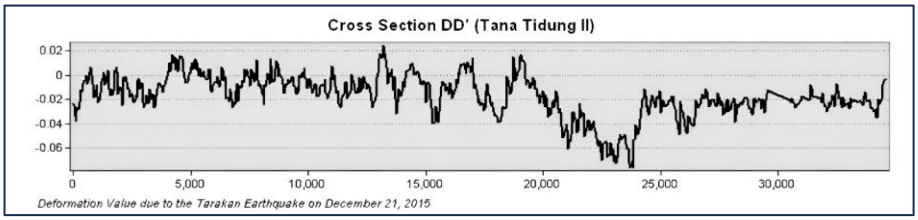

Source: Analysis, 2025

Figure 12. Vertical Cross-section Graph of DD' in Tana Tidung II Regency

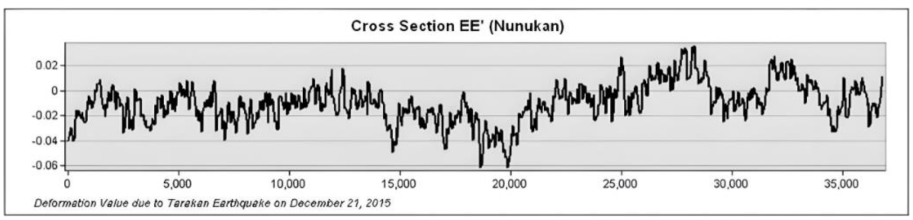

Source: Analysis, 2025

Figure 13. Vertical Cross-section Graph of EE' in Nunukan Regency

Figure 12 illustrates the cross-section graph of the northwest-southeast cross section in the Tana Tidung II Regency area, where the Tarakan earthquake occurred. The graph shows that uplift deformation dominates the east segment of this region. The uplift deformation value in this area ranges from 0.001 to 0.069 meters. The largest uplift deformation value is found 10 kilometers north of the earthquake's epicenter. Nunukan Regency's Southwest-Northeast (EE') cross section (Figure 13) shows uplift deformation in the southwest and subsidence in the northeast. The uplift deformation range is 0.001–0.062 meters, whereas the subsidence deformation range is 0.001–0.029 meters. Maximum uplift and subsidence deformation values occur northwest of the earthquake's epicenter.

The surface deformation values due to the Tarakan earthquake on December 21, 2015 provide information on the seismic hazard in the North Borneo, especially in Tarakan City, Nunukan Regency, Bulungan Regency, Tana Tidung I Regency (southwest of the earthquake epicentre), and Tana Tidung II Regency (north of the earthquake epicentre). Previously thought to be an earthquake-safe region, this is no longer the case. The epicentre of the Tarakan earthquake, which was located far from the Tarakan Fault, provides evidence of other locally active faults. In the past year, the Indonesian Meteorology, Climatology and Geophysics Agency (BMKG) recorded several earthquakes in the North Borneo region. On August 10, 2024, at 16:20:23 WITA, an earthquake magnitudo M 4.6 occurred on land to the southeast of Tarakan City, precisely at 63 km southeast of Tarakan City, with a shallow depth of 11 km. The earthquake was felt by people in Tarakan City, Tanjung Selor Regency, Berau Regency, and Tana tidung Regency with an intensity scale of III-IV MMI (Mercally Modified Intensity). At this intensity scale, the earthquake was felt quite strongly by many people, the windows/doors rattled, and walls rang. The source of the fault that caused the earthquake was a locally active fault.

Subsidence and uplift deformation due to the earthquake through the DInSAR method successfully identified the fault slip characteristics that caused the Tarakan earthquake on December 21, 2015. Figure 3 is the focal mechanism of the Tarakan earthquake obtained from the Global CMT catalogue. The focal mechanism parameters show the strike, dip and slip values of two fault planes, where only one fault plane is selected as the main fault plane. Research that has been conducted on the distribution of aftershocks from the Tarakan earthquake, shows the earthquake slip moves from the epicentre of the main earthquake to the south (Sriyanto et al. 2016). Based on the results of this study, the main fault plane that caused the Tarakan earthquake has a strike value: 3^{o}, dip: 86^{o}, and slip: 169^{o}. The strike, dip, and slip values represent the hanging wall of the fault to the west, and the foot wall of the fault to the east. The slip value on the fault indicates that the fault has an oblique fault mechanism dominated by strike-slip movement. The results of SAR image processing using the DInSAR method, which shows the surface deformation caused by the Tarakan earthquake (Figure 8), show that the area east of the epicentre of the earthquake (parts of the eastern part of Tana Tidung II Regency and Bulungan Regency) experienced uplift deformation (red colour), and the area west of the epicentre (the western part of Tana tidung II Regency, Nunukan Regency, and Tarakan City) experienced subsidence deformation (blue colour). There is a correspondence between the source of the Terakan earthquake and the surface deformation caused by the Tarakan earthquake. The characteristics of the fault that caused the Tarakan earthquake are oblique-normal faults dominated by strike-slip fault movements and normal (downward) fault blocks located to the west. The downward movement of the main fault plane to the west of the epicentre of the Tarakan earthquake corresponds to the record of the greatest level of shaking and damage caused by the earthquake, namely Tarakan City and Nunukan Regency on the IV-V MMI shaking level scale.

Subsidence and uplift deformation will certainly have an impact on the damage to buildings and other infrastructure. Earthquake preparedness strategies need to be known by the community and local government in areas prone to subsidence and uplift. Moreover, the geological structure in the Borneo region can exacerbate the value of subsidence and uplift. The geological structure of North Borneo, which is dominated by alluvium deposits and sedimentary rocks, contributed to the land surface deformation that occurred in various regions near the epicenter of the Tarakan earthquake on December 21, 2015. Alluvium deposits and sedimentary rocks are very soft structures, causing seismic waves to flow more slowly, resulting in larger earthquake shocks. Several measures can be taken by the community and local government to reduce the risk of disasters caused by earthquakes, including ensuring that buildings where people live or work have structures that are resistant to earthquake shocks, and are not located close to highlands such as hills, because changes in earthquake deformation can cause landslides.

4. Conclusion

The interferogram produced by the Tarakan earthquake on December 21, 2015, focuses on the primary earthquake in the North-Northeast, Southeast-Southwest, and Southwest-Northwest directions. The Tarakan earthquake caused the highest land rise (uplift) deformation value of 0.117618 meters, as well as the highest land subsidence deformation value of 0.0649612 meters. Both of these deformations happen around the main earthquake. Northwest-southeast cross sections were taken in Tarakan City, Tana Tidung I, Bulungan, and Tana Tidung II districts. A cross-section graph showing a northwest-southeast cross section in the Tana Tidung I area, 33 kilometers southwest of the earthquake epicenter, shows considerable uplift deformation of 0.019 to 0.079 meters. Significant uplift deformation in the Bulungan Regency area, which is approximately 11 kilometers southeast of the earthquake epicenter, ranges between 0.008 and 0.075 meters. The Tana Tidung II Regency area, which is the epicenter of the Tarakan earthquake, shows that uplift deformation dominates the southeast half of the region. The uplift deformation value in this area ranges between 0.001 and 0.069 meters. The maximum uplift deformation value occurs 10 kilometers north of the earthquake's epicenter.

The cross-section graph of Nunukan Regency from southwest to northeast indicates uplift deformation in the southwest and subsidence in the northeast. The uplift deformation range is 0.001-0.062 meters, and the subsidence deformation range is 0.001-0.029 meters. The highest uplift and subsidence deformation values occur northwest of the earthquake's epicenter. The surface deformation values due to the Tarakan earthquake on

December 21, 2015 provide information on the seismic hazard in the North Borneo, and provide evidence of other locally active faults. Uplift deformation due to the Tarakan earthquake on December 21, 2015 occurred more to the east of the epicentre, while subsidence deformation occurred more to the west. This is consistent with the focal mechanism of the Tarakan earthquake, which indicates oblique-normal faults, with strike-slip fault movements dominating, and normal (downward) fault blocks located to the west. The geological structure of North Borneo, which is dominated by alluvium deposits and sedimentary rocks, causes seismic waves to flow more slowly, resulting in greater earthquake shaking, which can increase ground surface deformation.

5. References

Azhari, M F, Karyanto, K., Rasimeng, S., & Mulyanto, B. S. (2020). Analysis of surface deformation using dinsar method (differential interferometry synthetic aperture radar) in case study lombok earthquakes on august 2018. *J. Geof. Ekspl*, *6*, 131-144.. [Crossref]

ASF HyP3 Sentinel-1 Burst InSAR Product Guide. URL https://hyp3-docs.asf.alaska.edu/hyp3-docs/guides/burst_insar_product_guide/

Balaguru, A., Nichols, G., & Hall, R. (2003). The origin of the'circular basins' of Sabah, Malaysia.

Badan Meteorologi Klimatologi Geofisika (BMKG) Data Catalog. URL https://bmkg.go.id

Bedini, Bedini, E. (2020). Persistent Scatterer Interferometry of Sentinel-1 time series to detect ground subsidence in the city of Recife, Brazil. *Journal of Hyperspectral Remote Sensing*, *10*(1), 1–9. https://doi.org/10.29150/jhrs.v10.1.p1-9. [Crossref]

Braun, A., & Veci, L. (2020). Sentinel-1 toolbox TOPS interferometry tutorial. *Waterloo, ON, Canada: European Space Agency*.

Cahyaningrum, A. P., (2024). Analisis Deformasi Berbasis Citra SAR. Pelatihan Teknis Analisis Data Science BMKG

Calvet, A., Balbarani, S., & Gende, M. (2023). DinSAR coseismic deformation measurements of the Mw 8.3 Illapel earthquake (Chile). *Journal of Geodetic Science*, *13*(1), 20220154.[Crossref]

Campbell, J. B., & Wynne, R. H. (2011). *Introduction to remote sensing*. Guilford press.

Castaneda, C., Pourthie, N., & Souyris, J. C. (2011). Dedicated SAR interferometric analysis to detect subtle deformation in evaporite areas around Zaragoza, NE Spain. *International Journal of remote sensing*, *32*(7), 1861-1884.[Crossref]

Center of Earthquake and Tsunami BMKG., (2016). Buletin Gempabumi dan Tsunami Indonesia Tahun 2015. Book ISSN: 2477 – 0035.

Erdi, A., Jackson, C. A. L., & Soto, J. I. (2023). Extensional deformation of a shale-dominated delta: Tarakan Basin, offshore Indonesia. *Basin Research*, *35*(3), 1071-1101.[Crossref]

Fahrland, E., Jacob, P., Schrader, H., & Kahabka, H. (2020). Copernicus digital elevation model product handbook. *Airbus Defence and Space—Intelligence: Potsdam, Germany*.

Gabriel, A. K., Goldstein, R. M., & Zebker, H. A. (1989). Mapping small elevation changes over large areas: Differential radar interferometry. *Journal of Geophysical Research: Solid Earth*, *94*(B7), 9183-9191.[Crossref]

Global Centroid-Moment Tensor Catalog Web Search. URL https://www.globalcmt.org/CMTsearch.html.

Gorsel, J. T. V. (2018). Bibliography of the Geology of Indonesia and Surrounding Areas, IV. Borneo (incl. Makassar Straits) 7.0. www.vangorselslist.com

Gourmelen, N., Amelung, F., & Lanari, R. (2010). Interferometric synthetic aperture radar–GPS integration: Interseismic strain accumulation across the Hunter Mountain fault in the eastern California shear zone. *Journal of Geophysical Research: Solid Earth*, *115*(B9).[Crossref]

Govil, H., & Guha, S. (2023). Underground mine deformation monitoring using Synthetic Aperture Radar technique: A case study of Rajgamar coal mine of Korba Chhattisgarh, India. *Journal of Applied Geophysics*, *209*, 104899.. [Crossref]

Gürpinar, A., Serva, L., Livio, F., & Rizzo, P. C. (2017). Earthquake-induced crustal deformation and consequences for fault displacement hazard analysis of nuclear power plants. *Nuclear Engineering and Design*, *311*, 69-85. [Crossref]

Hall, R. (2013). Contraction and extension in northern Borneo driven by subduction rollback. *Journal of Asian Earth Sciences*, *76*, 399-411.[Crossref]

Hall, R. (2019). The subduction initiation stage of the Wilson cycle..” [Crossref]

Hanifa, R. N., Anantasena, Y., Sadly, M., & Ito, T. (2019, June). Ground deformation identification related to 2018 lombok earthquake series based on Sentinel-1 data. In *IOP Conference Series: Earth and Environmental Science* (Vol. 280, No. 1, p. 012004). IOP Publishing. [Crossref]

Hendardi, R. P., Hidajat, W. K., Setyawan, R., Kurniasih, A., Qadaryati, N., Khorniawan, W. B., ... & Ringga, A. G. (2024). Evaluation of Reservoir Characteristics of Wells X, Y, Z in the Pliocene Interval of the Tarakan Sub-Basin, Tarakan Basin, North Kalimantan. *Journal of Applied Geology*, *9*(2), 126-138.. [Crossref]

Hogenson, K., Arko, S. A., Buechler, B., Hogenson, R., Herrmann, J., & Geiger, A. (2016, December). Hybrid Pluggable Processing Pipeline (HyP3): A cloud-based infrastructure for generic processing of SAR data. In *Agu fall meeting abstracts* (Vol. 2016, pp. IN21B-1740).[Crossref]

Indonesia Geospasial: Sistem Informasi Geografi dan Penginderaan Jauh., (2020). Shapefile (SHP) Geologi Provinsi Borneo Utara. URL https://www.indonesia-geospasial.com/2020/03/download-data-shapefile-shp-geologi-se.html.

Islam, L. J. F., Prasetyo, Y., & Sudarsono, B. (2017). Analisis penurunan muka tanah (Land subsidence) kota semarang menggunakan citra sentinel-1 berdasarkan metode dinsar pada perangkat lunak SNAP. *Jurnal Geodesi Undip*, *6*(2), 29-36.[Crossref]

Jaya, L. M. G., Simatupang, M., Kadir, A., & Saleh, F. (2021). Using DInSAR to map ground deformation on road infrastructure (case study: North Buton, Southeast Sulawesi). In *IOP Conference Series: Earth and Environmental Science* (Vol. 871, No. 1, p. 012019). IOP Publishing.[Crossref]

Jiang, X., Min, X., Ye, T., Li, X., & Hu, X. (2023). Monitoring the subsidence at different periods in high underground water level coal mine areas using differential interferometric synthetic aperture radar (D-InSAR). *Geocarto International*, *38*(1), 2215730.. [Crossref]

Kurniawan, R., & Anjasmara, I. M. (2016). Pemanfaatan Metode Differential Intermerometry Synthetic Aperture Radar (DInSAR) untuk Pemantauan Deformasi Akibat Aktivitas Eksploitasi Panasbumi. *Jurnal Teknik ITS*, *5*(2), B331-B336.

Lu, C. H., Huang, S. Y., Hsu, Y. C., Yen, I. C., Tung, H., & Kuo, Y. T. (2025). Fast report: the 2025 M6. 4 Dapu earthquake: preliminary field observation and surface deformation analysis. *Terrestrial, Atmospheric and Oceanic Sciences*, *36*(1), 14.[Crossref]

Manconi, A. (2021). How phase aliasing limits systematic space-borne DInSAR monitoring and failure forecast of alpine landslides. *Engineering Geology*, *287*, 106094.[Crossref]

Nasa's Earth Science Data System (ESDS). https://www.earthdata.nasa.gov/.

North Borneo Regional Disaster Management Agency. URL https://kaltim.tribunnews.com

Panuntun, H., Miyazaki, S. I., Fukuda, Y., & Orihara, Y. (2018). Probing the Poisson's ratio of poroelastic rebound following the 2011 M w 9.0 Tohoku earthquake. *Geophysical Journal International*, *215*(3), 2206-2221.[Crossref]

Permana, A. K., Sendjaja, Y. A., Panggabean, H., & Fauzely, L. (2018). Depositional Environment and Source Rocks Potential of the Miocene Organic Rich Sediments, Balikpapan Formation, East Kutai Sub Basin, Kalimantan. *Jurnal Geologi dan Sumberdaya Mineral*, *19*(3), 171-186.[Crossref]

Petersen, M. D., Dawson, T. E., Chen, R., Cao, T., Wills, C. J., Schwartz, D. P., & Frankel, A. D. (2011). Fault displacement hazard for strike-slip faults. *Bulletin of the Seismological Society of America*, *101*(2), 805-825.[Crossref]

Purba, J., Priadi, R., Amelia, R., Dwilyantari, A. A. I., Jaya, L. M. G., Ode Restele, L., & Gana Putra, I. (2024). Surface deformation and its implications for land degradation after the 2021 Flores earthquake (M7. 4) using differential interferometry synthetic aperture radar. *Journal of Degraded & Mining Lands Management*, *12*(1).[Crossref]

Purba, S. M., Alyssa, Y. F., Nadia, M., Asra, N., & Muksin, U. (2025, April). The Influence of Seismometer Coverage on the Earthquake Focal Mechanism Solution (Case Study: Toba Swarm Earthquake). In *IOP Conference Series: Earth and Environmental Science* (Vol. 1479, No. 1, p. 012014). IOP Publishing.[Crossref]

Puspita, A., Pertiwi, I. I., & Sinki, K. P. (2024, July). Surface deformation analysis due to the Poso earthquake on May 29, 2017 using the DInSAR method. In *IOP Conference Series: Earth and Environmental Science* (Vol. 1373, No. 1, p. 012049). IOP Publishing.[Crossref]

Sari, A. R., Handayani, H. H., & Agustan, A. (2014). Penerapan metode Dinsar untuk analisa deformasi akibat gempa bumi dengan validasi data GPS Sugar (Studi kasus: Kepulauan Mentawai, Sumatera Barat). *Geoid*, *10*(1), 26-31. https://journal.its.ac.id/index.php/geoid/article/view/1431

Souza, W. D. O., de Moura Reis, L. G., da Silva Pereira Cabral, J. J., Ruiz-Armenteros, A. M., Quental Coutinho, R., da Penha Pacheco, A., & Ramos Aragão Junior, W. (2024). Analysis of Urbanization-Induced Land Subsidence in the City of Recife (Brazil) Using Persistent Scatterer SAR Interferometry. *Remote Sensing*, *16*(14), 2592.

Sriyanto, S. P. D., & Ifantyana, I. (2016). Identifikasi Patahan Mikro Penyebab Gempa Bumi Tarakan 21 Desember 2015. In *Prosiding Seminar Nasional Fisika, V, SNF2016-EPA-79-SNF2016-EPA-84*.[Crossref]

Téllez-Quiñones, A., Salazar-Garibay, A., Valdiviezo-Navarro, J. C., Hernandez-Lopez, F. J., & Silván-Cárdenas, J. L. (2020). DInSAR method applied to dual-pair interferograms with Sentinel-1 data: a study case on inconsistent unwrapping outputs. *International Journal of Remote Sensing, 41*(12), 4664-4683.[Crossref]

Téllez-Quiñones, A., Salazar-Garibay, A., Cruz-Sánchez, B. I., Carlos-Martínez, H., Valdiviezo-Navarro, J. C., & Soto, V. (2025). Three-Dimensional Ice-Flow Recovery from Ascending–Descending DInSAR Pairs and Surface-Parallel Flow Hypothesis: A Simplified Implementation in SNAP Software. *Remote Sensing, 17*(7), 1168. [Crossref]

Watkinson, I. M., & Hall, R. (2017). Fault systems of the eastern Indonesian triple junction: evaluation of Quaternary activity and implications for seismic hazards.[Crossref]

Witts, D., Hall, R., Nichols, G., & Morley, R. (2012). A new depositional and provenance model for the Tanjung Formation, Barito Basin, SE Kalimantan, Indonesia. *Journal of Asian Earth Sciences, 56*, 77-104.[Crossref]